Implementation of Dynamic Material Property Data in Finite-Element Modeling Simulations

J. Heigel*, R. Ivester, E. Whitenton
National Institute of Standards and Technology[a], Gaithersburg, Maryland, 20899-8223 USA
*jarred.heigel@nist.gov

Abstract
This paper presents a method of implementing dynamic material properties obtained through pulse-heated Kolsky bar (Split-Hopkinson bar) experimentation into commercially available finite-element simulation software for cutting processes. Material property experiments performed at high strain-rates and high initial temperatures obtain a closer approximation to the conditions experienced during metal cutting than could be achieved with traditional material property testing. However, difficulty exists in implementing the data obtained from the Kolsky bar experiments into existing cutting simulation software. This paper presents a methodology for incorporating dynamic material property data into cutting simulation software. First, software used for cutting simulations simulates Kolsky bar experiments. These simulations allow adjustment of the material model parameters to bring experimental and simulated true-stress true-strain curves into agreement. Finally, results from 2D orthogonal cutting simulations using the new material model parameters are verified using measurements made with a dual-spectrum high-speed microvideography system and comparable simulations performed with the default material model parameters.

1. INTRODUCTION

Finite-element analysis (FEA) provides an effective method for academia and industry to study the metal cutting process. Areas of interest include cutting forces, temperatures [1, 2], chip formation (segmentation, curl, and breakage) [3, 4], and residual workpiece properties [5, 6]. Simulation results of these phenomena rely on the chosen material model and associated material parameter values.

Most FEA users utilize commercially available modeling packages that allow the control of the material property parameters that fit into the implemented model framework. Proprietary models result in ambiguity for the user concerning the effect of the material property parameters on model accuracy. In addition, the lack of reliable data at the extreme strains, strain-rates, and temperatures experienced during metal cutting make it difficult for the user to create application specific FEA material model parameters that represent the chosen real-world material. Furthermore inconsistencies between batches of the same material and variations of material properties with a single workpiece resulting from initial processing methods (rolling, drawing, casting, etc.) make it difficult to apply one set of material property parameters for a desired workpiece material. A simple illustration of this variation within a single workpiece can be seen in Figure 1 where the hardness increases as the measurements are made closer to the surface. This same behavior can be expected when considering more complex material properties such as grain sizes and phases, residual stresses, and chemical distributions within the material.

To accommodate differences in material properties available to the user, the most common practice involves performing a range of cutting experiments and simulations. The simulation results are compared to the experimental cutting results and the FEA material model properties are adjusted to achieve a match. This

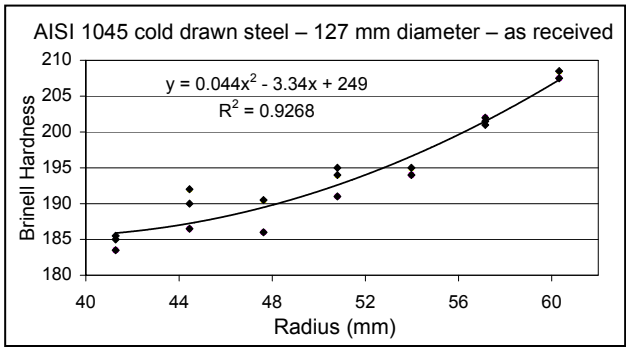

Figure 1. Hardness variation with a single workpiece of material.

[a] This paper is an official contribution of the National Institute of Standards and Technology and is not subject to copyright in the United States.

process can yield adequate results, but at significant cost due to the amount of time required for a cutting simulation to achieve steady state and the production resources devoted to providing the reference data.

A more efficient, science-based approach involves using the results of dynamic material property tests at high temperatures and strain-rates to adjust the material model property data. The work presented in this paper uses a Kolsky bar at the National Institute of Standards and Technology (NIST) to perform high strain-rate, pulse heated material property tests [7]. This method achieves strain-rates and temperatures closer to the values experienced during metal cutting than in traditional material property testing methods [8, 9].

This data is implemented into an existing commercial analysis package, Third Wave Systems' AdvantEdge[b] [10]. The package is used to simulate the Kolsky bar experiments to obtain a direct comparison between measured and simulated material properties. This method removes difficulty of determining material properties from metal cutting experiments, which do not provide a direct measure of material properties. Adjusting the simulation material model parameters brings the simulated true-stress true-strain curves into agreement with the curves obtained from the Kolsky bar experiments. A comparison between simulated two-dimensional (2-D) cutting results and experimentally obtained cutting forces and chip temperatures provides a method of assessing the ability to implement the dynamic material property data into the material model parameters. American Iron and Steel Institute (AISI) 1045 steel disks cut while measuring the forces using a multi-axis dynamometer, and the chip temperature using the NIST dual-spectrum high-speed microvideography setup [11, 12], provide reference cutting data.

2. KOLSKY BAR EXPERIMENTS

The Kolsky bar facility at NIST utilizes the principles of a Split Hopkinson Pressure Bar [13] in conjunction with pulse heating to obtain dynamic material properties at high strain-rates (≈6000 s^{-1}), temperatures (20 °C to 1200 °C), and heating rates (≈1200 °C/s) to gain a better understanding of material properties during metal cutting. An electric current is applied to the sample to quickly heat the sample before deformation occurs. This high heating rate before deformation allows the assumption of minimal micro-structural changes in the workpiece material during the heating process.

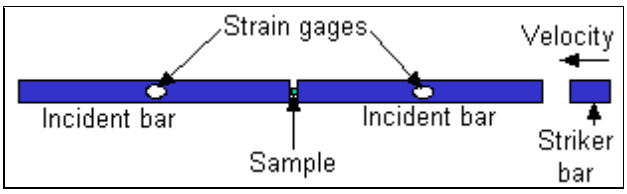

Figure 2. Kolsky bar setup

2.1 Kolsky Bar setup

Figure 2 illustrates the Kolsky apparatus. A 4 mm diameter, 2 mm thick sample is placed between two bars. Pulse heating brings the workpiece to the desired temperature in less than 1 s. Once the workpiece reaches uniform temperature, one incident bar is struck with a velocity up to 600 m/min. This causes the bar to compress the sample at a high rate against the other bar. Strain gauges mounted to the bars provide compression data while a pyrometer provides workpiece temperature data.

2.2 Acquired true-stress, true-strain

Figure 3 provides raw true-stress true-strain curves of AISI 1045 steel samples obtained through Kolsky bar tests. The average strain rate and initial sample temperature labels each curve. Non-equilibrium at impact requires the data at the beginning of the curve to be disregarded until the compression reaches equilibrium. No uncertainty analysis has been performed on this raw data.

Later sections of this paper present a detailed analysis of these curves in the context of the

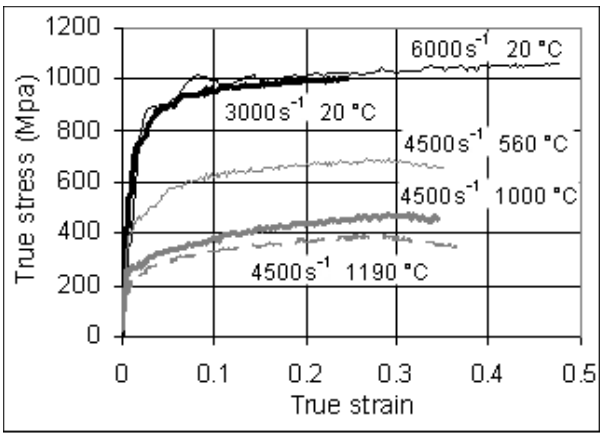

Figure 3. Stress-strain curves obtained from Kolsky bar experiments.

[b] Commercial equipment and materials are identified in order to adequately specify certain procedures. In no case does such identification imply recommendation or endorsement by the National Institute of Standards and Technology, nor does it imply the materials or equipment are necessarily the best available for the purpose.

simulation material model parameters. However, note the following: 1) the top two curves of the same initial temperature show a small strain rate sensitivity (increasing flow stress with increasing strain rate) at these strain rates and 2) a seemingly linear behavior appears evident in the thermal softening effect from 20 °C to 1190 °C (decreasing flow stress with increasing initial temperature).

3. KOLSKY BAR SIMULATIONS

The commercial FEA software used to simulate metal cutting can be used to model the Kolsky bar experiments. This allows a better understanding of the material model parameters used. Furthermore, it enables implementation of experimentally derived properties from the Kolsky bar into the metal cutting material model parameters. This allows greater confidence that the simulation material property parameters provide a simulation which more accurately represents the real-world material.

3.1 Simulation setup

The "2-D orthogonal cutting" feature of the FEA software allows simulations to deform 2 mm x 4 mm workpieces using a neutral rake tool significantly larger than the workpiece. Figure 4 shows workpiece and tool constraints. A friction parameter value of 0.01 describes the friction between the tool and workpiece. This low value is necessary for two reasons: 1) lubrication is implemented in all Kolsky bar experiments, significantly reducing friction, 2) effects of material property parameters are the desired results of the simulation. A low friction parameter minimizes the effects of friction.

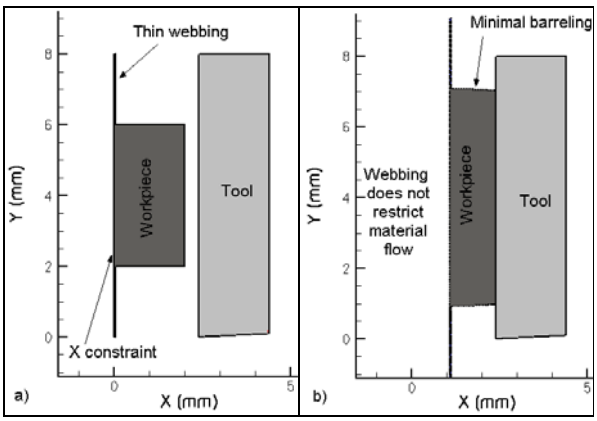

Figure 4. Simulation setup a) before deformation and b) after deformation.

3.2 Material model

AdvantEdge allows the definition of custom materials through properties in five areas (Table 1). Published data on AISI 1045 steel for this application define the heat transfer and elastic parameters [14]. Basic material property tests can be used to define these parameters in the absence of published reference data.

3.3 Defining parameters

Assuming little or no interdependence between

Parameter	Symbol	Final value	Unit	Source
Heat transfer parameters				
Thermal conductivity	*k*	51.9	W / (m · °C)	taken from published values
Heat capacity	*c*	486	J / (kg · °C)	taken from published values
Density	*den*	7870	kg / m^3	taken from published values
Strain Hardening parameters				
Initial yield stress	*sg0*	3.7E+08	Pa	iterated until stress strain graphs matched
Initial plastic strain	*ep0*	0.05	-	iterated until stress strain graphs matched
Strain hardening exponent	*En*	8	-	iterated until stress strain graphs matched
Strain hardening cutoff	*epc*	1	-	iterated until stress strain graphs matched
Thermal softening parameters				
Polynomial coefficient	*C0*	1.0109	-	taken directly from plot of Kolsky bar data
Polynomial coefficient	*C1*	-5.4623E-04	-	taken directly from plot of Kolsky bar data
Polynomial coefficients	*C2, C3, C4, C5*	0	-	taken directly from plot of Kolsky bar data
Reference temperature	*Tr*	20	°C	taken directly from plot of Kolsky bar data
Melting temperature	*Tm*	1540	°C	taken from published values
Cutoff temperature	*Tc*	1200	°C	taken directly from plot of Kolsky bar data
Strain rate sensitivity parameters				
Low rate exponent	*m1*	29	-	matched AdvantEdge produced graph to graph of Kolsky data
High rate exponent	*m2*	29	-	matched AdvantEdge produced graph to graph of Kolsky data
Reference plastic strain rate	*epr*	9E-04	s^{-1}	matched AdvantEdge produced graph to graph of Kolsky data
Threshold strain rate	*prt*	1E+07	s^{-1}	matched AdvantEdge produced graph to graph of Kolsky data
Elastic parameters				
Young's modulus	*Ey*	2E+11	Pa	taken from published values
Poisson's ratio	*Pr*	0.29	-	taken from published values

Table 1. AdvantEdge material model parameters with the final values used by NIST.

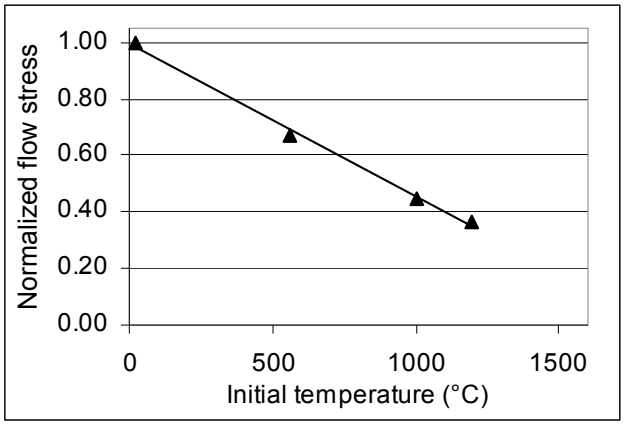

Figure 5. Kolsky bar derived thermal softening.

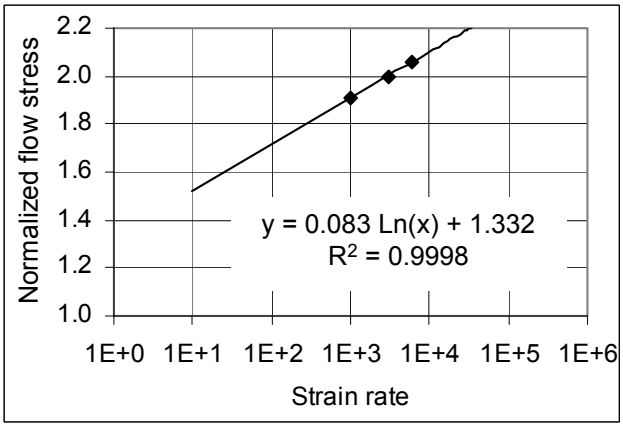

Figure 6. Kolsky bar derived strain rate sensitivity.

thermal softening, strain rate sensitivity, and strain hardening allows independent determination of each area's parameters. We use a strain of 0.24 as the point of comparison during analysis.

Thermal softening

Figure 5 illustrates the convention for defining thermal softening. This method normalizes the flow stresses by the flow stress found at an initial temperature of 20 °C, thus providing a direct comparison to the graph generated by Advantedge during material parameter selection. The Kolsky bar data shows a predominately linear behavior up to the maximum tested initial temperature of 1190 °C allowing the implementation of a linear model. *Tc* represents the maximum temperature defined by the linear fit. The behavior up to the melting temperature, *Tm* (from published data), is defined automatically by the software using linear interpolation between *Tc* and *Tm*.

Strain rate sensitivity

Figure 6 represents the strain hardening effect with flow stress normalized by a reference stress at a strain rate of 1 s^{-1}. Published yield and ultimate stresses provide the upper and lower bounds to infer the reference stress at 0.24 strain. We vary the material parameters until the Advantedge produced curve matches the curve derived from the Kolsky bar data.

Strain hardening

An iterative process determines the strain hardening parameters by performing simulations at a similar strain rate and initial temperature as a Kolsky bar experiment curve. In this case, the curve from 6000 s^{-1} at an initial temperature of 20 °C provides the comparison point. Simulations of the Kolsky bar experiments require an order of magnitude less time than simulations of cutting experiments, making the iterative process acceptable.

3.4 Kolsky simulation results

Figure 7 presents a comparison of the Kolsky bar simulation results to the Kolsky bar experimental results. Curves labeled X represent data at 6000 s^{-1} and 20 °C, curves labeled Y represent data at 3000 s^{-1} and 20 °C, and curves labeled Z represent data at 4500 s^{-1} and 1000 °C.

Simulations using default parameters vs. measured experimental data

The curves in Figure 7a and Figure 7b show that the room temperature (20 °C) flow stresses predicted using the default parameters are too high, but achieve a closer approximation at the elevated temperature (1000 °C). The strain rate sensitivity, represented by the difference between curves X and Y, is similar to that observed in the experimentally obtained curves. The strain hardening effect is too high in the default simulation curves at room temperature. However, the strain hardening effect at the higher temperature test more closely represents the experimentally measured result.

Simulations using custom parameters vs. measured experimental data

Figure 7c shows the simulation results when using final custom material property parameters to represent our AISI 1045 steel samples. These curves show a better relationship between the average simulated curve stress values at each temperature and strain rate.

Figure 8 provides a more detailed comparison between the simulations using custom material property parameters and the measurements from Kolsky bar experiments. The plots in Figure 7 posess the same range (200 MPa and 0.5 strain) on each axis, allowing the slopes (strain hardening effect) of the curves to be

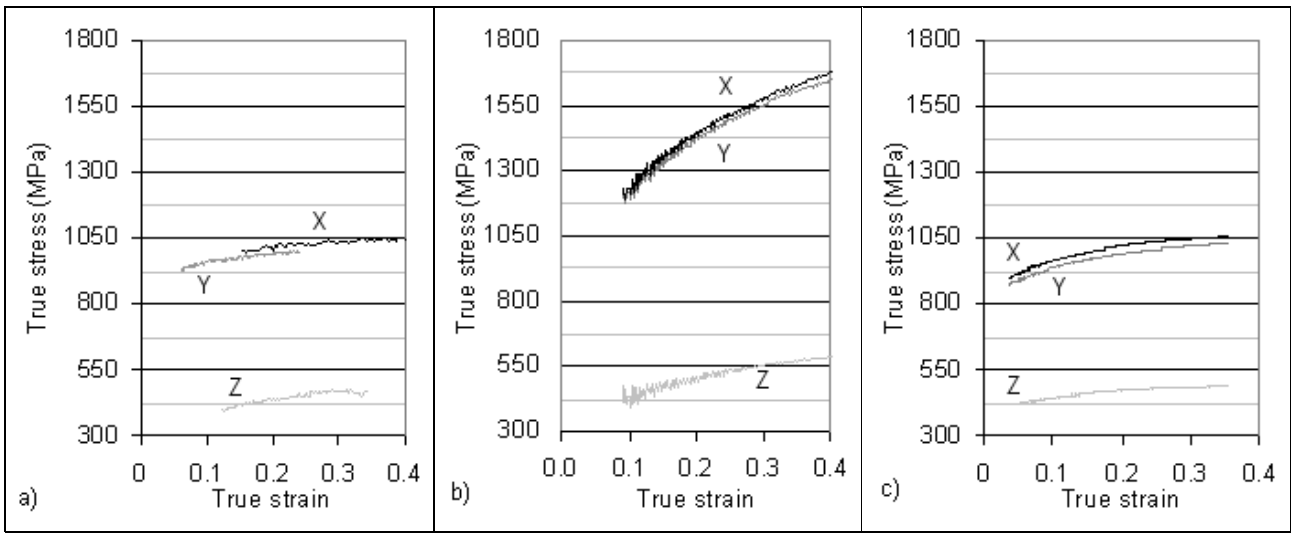

Figure 7. Results from a) Kolsky bar experiments, b) simulations using default material property parameters, and c) simulations using custom material property parameters.

compared. The simulated curves in Figure 8a and Figure 8b show nearly identical strain hardening. However, the simulated curve in Figure 8c displays a significantly different strain hardening behavior. This suggests an interdependency between thermal softening and strain hardening in the simulation software material model.

4. COMPARISON TO MEASUREMENTS DURING ORTHOGONAL CUTTING

Dual-spectrum high-speed microvideography provides metal cutting data consisting of forces, temperature, and chip flow/formation during orthogonal cutting. Cutting with two inserts, a TNMG220408-MR4 insert held at a -7° rake and an A4G0605M06U04B insert held at a +5° rake, both cutting disks at a feed of 0.3 mm per revolution provides diverse cutting conditions to test the robustness of the material property parameters.

4.1 Force and temperature

Prior work describes the temperature measurement method and results for a single tool [12]. However, the current analysis uses a simpler approach, only considering the peak temperature in the chip for multiple tools. Comparisons between measurement and simulation results are made using the average steady state values of cutting force, thrust force, and peak temperature. Table 2 presents a comparison between measured and simulated cutting results using both the software's default "AISI 1045 200 Bhn" and custom material properties.

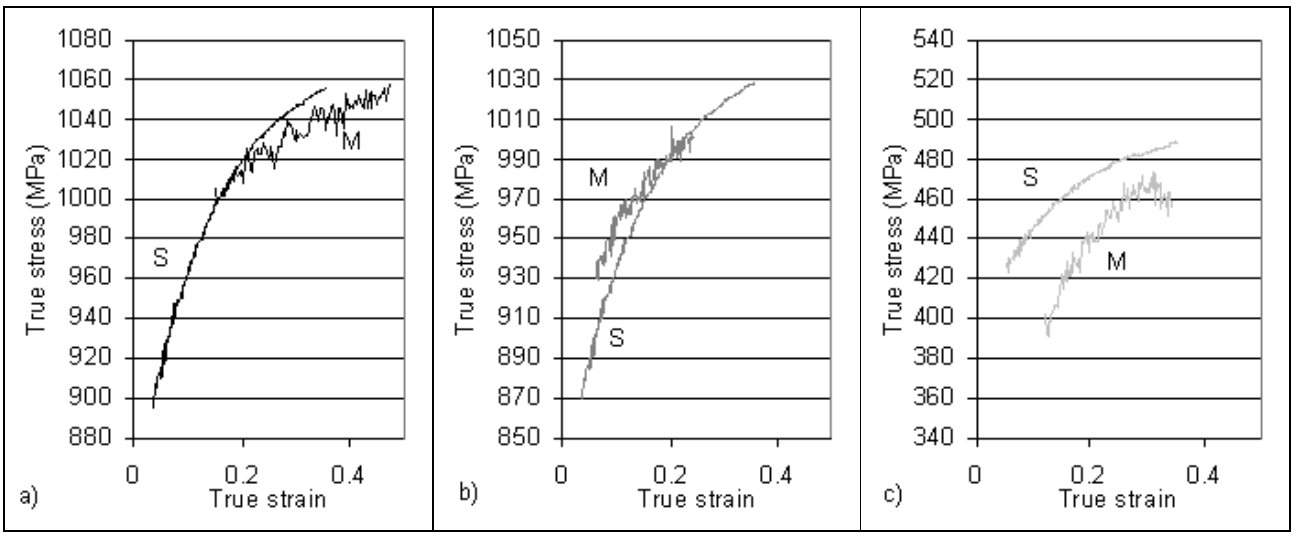

Figure 8. Comparison of Kolsky bar experiment measurements (M) and Kolsky bar simulations (S) for a) 6000 s-1, 20 °C, b) 3000 s-1, 20 °C, and c) 4500 s-1, 1000 °C.

Rake angle °	Surface speed m/min	Feed per revolution mm	Forces Cutting N	Forces Thrust N	Avgerage peak temperature °C Lower bound	Avgerage peak temperature °C Upper bound
Dual-spectrum microvideography measurements						
5	200	0.30	1672 ± 48	746 ± 42	785	1109
5	400	0.30	1575 ± 24	578 ± 14	793	1211
-7	250	0.30	1727 ± 137	892 ± 217	803	1211
-7	400	0.30	1725 ± 106	828 ± 153	961	1334
Simulation results using default AISI 1045 200 Bhn steel material properties						
5	200	0.30	1939 ± 10	287 ± 14	639	652
5	400	0.30	1860 ± 134	263 ± 51	785	817
-7	250	0.30	2092 ± 246	692 ± 126	757	776
-7	400	0.30	2002 ± 307	648 ± 133	839	878
Simulation results using material properties derived from Kolsky bar experiment simulations						
5	200	0.30	1799 ± 68	671 ± 45	627	653
5	400	0.30	1824 ± 20	666 ± 21	714	751
-7	250	0.30	1810 ± 18	863 ± 26	736	761
-7	400	0.30	1811 ± 14	850 ± 22	833	881

Table 2. Comparison between measured and simulated results.

The standard deviation of the force signal during steady state calculates the forces signal uncertainty. The expanded uncertainty with a coverage factor of 2 is expressed in the results [15]. Temperature uncertainty is mainly determined by the scatter in the data and the uncertainty of the emissivity value. Prior work analyzing a post-process chip calculated an emissivity value, *e*, of 0.46 with a standard uncertainty of 0.11 [12]. Figure 9 illustrates the upper and lower bounds on peak temperature as a result of emissivity uncertainty over the duration of a cutting test. Peak temperature uncertainty due to fluctuations in the signal is calculated using the standard deviation of the values during steady state and the expanded uncertainty is calculated using a coverage factor of 2. The total uncertainty of the peak temperature measurements displayed in Table 2 results from adding the expanded peak temperature fluctuation uncertainty to the upper and lower bounds defined by the emissivity uncertainty.

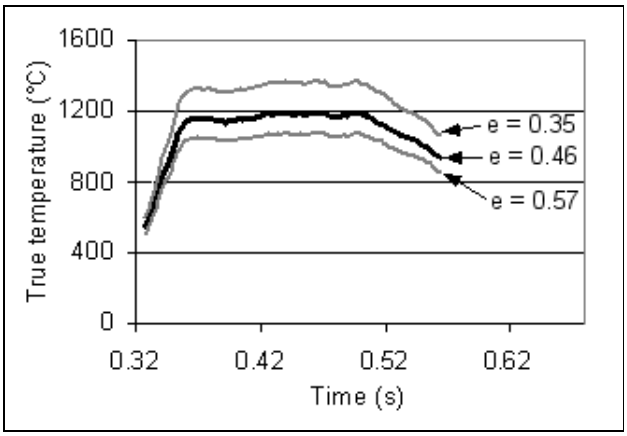

Figure 9. Example of the effect of emissivity on peak temperature calculations.

Rake angle °	Speed m/min	Feed mm/rev	Forces Cutting %	Forces Thrust %	Avg. peak temperature %
5	200	0.30	8.4	51.5	-0.6
5	400	0.30	2.3	39.4	-7.1
-7	250	0.30	16.3	19.2	-1.9
-7	400	0.30	11.1	19.3	-0.1

Table 3. Observed percent improvement over default material parameters for this study.

Table 3 illustrates the improvements made when developing material model parameters through Kolsky bar experiments and simulations. These improvements result from being able to characterize the properties of the exact material used, thus accounting for batch differences. Equation 1 calculates the percent improvements (*I*) where *M*, S_D, and S_C represent the average values of interest of the data created by experiments, simulations run using default material parameters, and simulations run using custom material parameters, respectively. Equation 1 works for average cutting force, average thrust force, and average peak temperature.

$$I = \frac{|M - S_D| - |M - S_C|}{|M|} * 100\% \quad (1)$$

The most noticeable difference between the default and the custom parameter simulations comes from the cutting and thrust forces becoming more representative of the measured forces. For this situation, the default parameter simulations consistently predict higher cutting forces and lower thrust forces, though on some occasions the force predictions and measurements are not significantly different. When observing the simulation data derived from custom material parameters based on Kolsky bar simulations, both the cutting and thrust forces are significantly closer to their measured counterparts. Negligible difference exists between the two simulation methods' average peak steady state temperatures and both are below the average measured value.

4.2 Chip flow

A high-speed visible light camera provides information on material flow and chip segmentation behavior. An earlier study by Ivester, et al. shows the -7° rake insert causes significant segmentation (Figure 10a) [11]. Thermal instability causing shear localization also appears in the infrared spectrum video (Figure 10b) presented by Heigel, et al [12]. Performing simulations with the default material parameters produces segmented chips (Figure 10c) in agreement with the evidence presented in the high-

speed video. However, when observing the simulations performed with the custom material parameters, no segmentation occurs (Figure 10d). The inability of the Kolsky bar experiments to capture the higher strain-rate behavior of the material during the cutting process prohibits shear localization in the simulation with the final custom material parameters.

Furthermore, the custom material parameters produce a larger chip curl radius and allow the chip material to engage the chip-breaker, whereas the default material parameters create a smaller radius curl and prevent the chip from engaging the chip breaker. Difficulty in assessing the observed experimental chip interaction with the chip breaker arises from resolution and field-of-view limitations, preventing the verification of the behavior in the visible light observations.

5. DISCUSSION

The results presented in this paper show the advantages of implementing dynamic material properties derived through Kolsky bar experiments in the FEA software for cutting analysis. Simulations of the Kolsky bar experiments provide a direct comparison method between simulated and measured true-stress, true-strain curves. This eliminates the ambiguity present when using cutting tests to estimate material model property parameters.

Kolsky bar experimental data directly determined the strain rate sensitivity and thermal softening effects. However, the strain hardening parameters relied on several iterations of the simulations of Kolsky bar experiments to achieve behavior that adequately matched the Kolsky bar experimental results. This iterative process requires significantly less time than the alternative method of iterating cutting simulations until the chosen parameters produce results matching those obtained from cutting experiments. Furthermore, this method does not require machine time to perform cutting tests, reducing the impact on a production facility while decreasing the time it takes to achieve a good material model for different workpiece materials.

Comparing simulation results derived using default and the custom material parameters to measurements made of orthogonal cutting processes show mixed results. Although the material property parameters derived in this study produce more representative cutting and

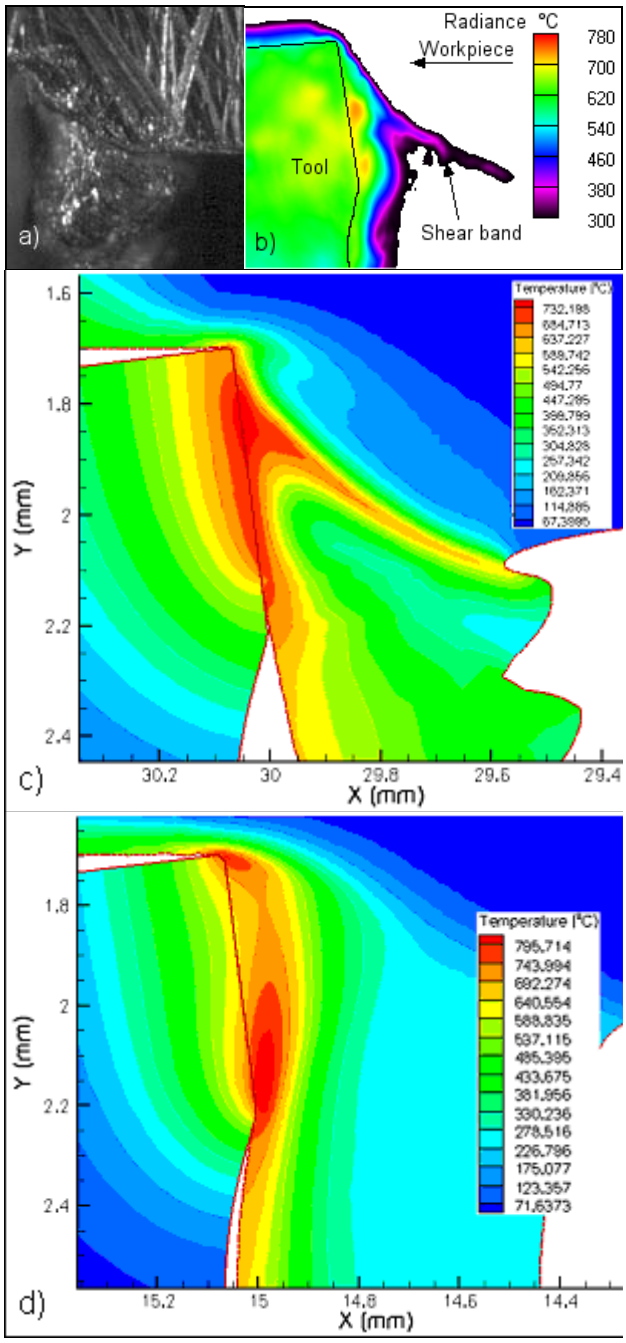

Figure 10. Chip formation images show segmentation from a) visible spectrum camera, b) thermal spectrum camera, c) default material parameter simulation, and d) custom material parameter simulation.

thrust forces of the selected workpieces, there is negligible change in the peak chip temperature and a poorer agreement in the chip morphology. This discrepancy in results could result from a lack of data at strain rates higher than 6000 s^{-1}.

This study shows the advantages of properly quantifying workpiece material properties at high strain rates and temperatures. By doing so, users can achieve a more efficient method

of implementing new materials into existing analysis packages. It is necessary to be able to implement new material property data into cutting simulation software to allow for the variation between batches of the same material. In addition, a single workpiece can vary significantly due to the initial processing technique, such as casting, rolling, or extruding. Moreover, the ongoing development of new workpiece materials requires the ability to adapt existing cutting simulation software to accurately predict the new material.

6. ACKNOWLEDGEMENTS

The authors acknowledge the support of Alkan Donmez, Hans Soons, Richard Rhorer, and Steve Mates of the National Institute of Standards and Technology. The authors would also like to thank the technical support staff of Third Wave Systems for their assistance.

7. REFERENCES

[1] Davies, M.A., Cau, Q., Cooke, A.L., Ivester, R.W., 2003, On the Measurement and Prediction of Temperature Fields in Machining AISI 1045 Steel, Annals of the CIRP, 52/1: 77-80.

[2] Meir, G., Hashemi, J., Chou, P.C., 1988, Finite-Element Simulation of Segmented Chipping in High-Speed Machining, Proceedings of Advanced Machining Technology II, SME, Phoenix, Arizona.

[3] Marusich, T.D., Brand, C.J., Thiele, J., 2002, A Methodology for Simulation of Chip Breakage in Turning Processes Using an Orthogonal Finite Element Model, Proceedings of the 5th CIRP International Workshop on Modeling of Machining Operations, 1/1: 139-148.

[4] Deshayes, L., Ivester, R.W., Mabrouki, T., Rigal, J-F., 2004, Serrated Chip Morphology and Comparison with Finite Element Simulations, Proceedings of the ASME Int. Mechanical Engineering Congress and Exposition, 1/1: 1-10.

[5] Jacobus, K.J., DeVor, R.E., Ka-poor, S.G., 1999, Part Warpage Model Based on Machining-Induced Residual Stress, Trans. of the North American Manufacturing Research Institution of SME, 27/1: 75-80.

[6] Marusich, T.D., Usui, S., McDaniel, J., 2003, Three-Dimensional Finite Element Prediction of Machining-Induced Stresses, Proceedings of the 2003 ASME Int. Mechanical Engineering Congress and Exposition, 1/1: 1-8.

[7] Burns, T.J., Mates, S.P., Rhorer, R.L., Whitenton, E.P., 2007, Recent Results from the NIST Pulse-Heated Kolsky Bar, Proceedings of the SEM Annual Conference and Exposition on Experimental and Applied Mechanics, Springfield, MA.

[8] Deshpande, A., Madhavan, V., Pednekar, V., Adibi-Sedeh, A.H., Ivester, R.W., 2006, Dependence of Metal Cutting Simulations on the Johnson-Cook Model Thermal Softening Parameter, Transactions of the North American Manufacturing Research Institution of SME, 34/1: 293-300.

[9] Jaspers, S.P.F.C., Dautzenberg, J.H., 2002, Material Behaviour in Conditions Similar to Metal Cutting: Flow Stress in the Primary Shear Zone, Journal of Materials Processing Technology, 122/2-3: 322-330.

[10] Marusich, T.D., Ortiz, M., 1995, Modelling and Simulation of High-Speed Machining, Int. Journal of Numerical Methods in Engineering, 38/21: 3675-3694.

[11] Ivester, R., Whitenton, E., Heigel, J., Marusich, T., Arthur, C., 2007, Measuring Chip Segmentation by High-Speed Microvideography and Comparison to Finite-Element Modeling Simulations, Proceedings of the 10th CIRP International Workshop on Modeling of Machining Operations, 1/1: 37-43.

[12] Heigel, J.C., Ivester, R.W., Whitenton, E.P., 2008, Cutting Temperature Measurements of Segmented Chips Using Dual-Spectrum High-Speed Microvideography, Transactions of the North American Manufacturing Research Institution of SME, 36/1: 73-80.

[13] Gray, G.T.I., 1998, Classic Split-Hopkinson Pressure Bar Testing, ASM Handbook 8, 1/1: 462-469.

[14] www.matweb.com.

[15] Taylor, B.N. Kuyatt, C.E., 1994, Guidelines for Evaluating and Expressing the Uncertainty of NIST Measurement Results, NIST Technical Note 1297.